Natural Hazards
and Earth System
Sciences

Open Access

EGU

Supplement of

Estimating network related risks: A methodology and an application in the transport sector

Jürgen Hackl et al.

Correspondence to: Jürgen Hackl (hackl@ibi.baug.ethz.ch) and Juan Carlos Lam (lam@ibi.baug.ethz.ch)

1 Introduction

This file provides supplementary information for the paper "Estimating network related risks: A methodology and an application in the transport sector". In this file, the models used for the risk assessment are explained in more detail. An overview of the models and their relationships are given in Figure 1. The models are described by six properties: Inputs, Outputs, Resources, Process, Calibration, Assumptions and limitations.

Inputs : The term "inputs" refers to those inputs that are provided by other modules in the simulation engine, or externally by the network manager.

Outputs : The term "outputs" refers to those outputs that are provided by the module and can be used by all other modules, or ultimately can be regarded to be the estimated consequences.

Resources : The term "resources" refers to model specific data, which is only needed by the current model and by none of the other models in the simulation engine. Dependent on the model used for a specific event, this data might change, e.g. while a simple traffic assignment model needs only the network and an origin-destination matrix, more complex models need additional (socio-demographic) data such as, housing and workplace locations, population and employment statistics, . . .

Process : This section gives a brief description of how the model is applied. Additionally, references to the original model is given.

Calibration : This section describes the process and data used to calibrate the models.

Assumptions and limitations : Since only simplified models are used in this example, some of the major underlying assumptions and limitations are listed in this section.

2 Modules

2.1 Rainfall

Inputs :
  T^{rain} – The return period desired to be investigated [years]. This input can be chosen by the network manager or determined by the desired return period T^{flood} of the flood event.

Outputs :
  $\boldsymbol{P}_{\tau^{\text{rain}}}$ – A time series of precipitation fields (i.e., raster file for every time step) over period τ, where each cell values $p_{\boldsymbol{c},t} \in \boldsymbol{P}_t$ with $t \in \tau^{\text{rain}}$ represented the rainfall intensity per time step [mm/hour].

Resources :
  $\mathcal{P}^{\text{rain}}$ – A precipitation catalogue of historical events, represented as a time series of precipitation fields over time, with a spatial resolution of $1\,\text{km} \times 1\,\text{km}$ and a temporal resolution of $1\,\text{hour}$. Source data was taken from Wüest et al. (2010).

Process : The first part of this process was choosing the time series of precipitation fields $\boldsymbol{P}_{\tau^{\text{rain}}} \in \mathcal{P}^{\text{rain}}$ to be used in a given simulation from the precipitation catalogue of Wüest et al. (2010). This involved two steps: (i) setting the beginning of the rainfall event from this catalogue using a simple random sampling algorithm, and (ii) selecting the duration of the rainfall event τ^{rain}.

The latter was accomplished using a simple random sampling algorithm on a scaled Beta probability distribution representing possible duration lengths, ranging from 1 to 72 hours. Each return period of interest had an assigned Beta probability distribution, with larger durations to be observed with higher frequency when modeling events of larger return periods. To further characterize a rainfall event, the second set of actions was needed to relate that event with a given return period. The precipitation values $p_{\boldsymbol{c},t} \in \boldsymbol{P}_{\tau^{\text{rain}}}$ for each raster cell $\boldsymbol{c}$ at time $t \in \tau^{\text{rain}}$ were iteratively scaled as described in Hackl et al. (2017) until the rainfall event generated a discharge value at a point of interest matching that of the desired return period. The result of this entire process was a time series of scaled precipitation fields $\boldsymbol{P}_{\tau^{\text{rain}}}$.

Finally, in order to match the spatial resolution to be used throughout the entire analysis (set at $16\,\text{m} \times 16\,\text{m}$), the resolution of all precipitation fields $\boldsymbol{P}_{\tau^{\text{rain}}}$ (originally set at $1\,\text{km} \times 1\,\text{km}$), was adapted using a regridding process.
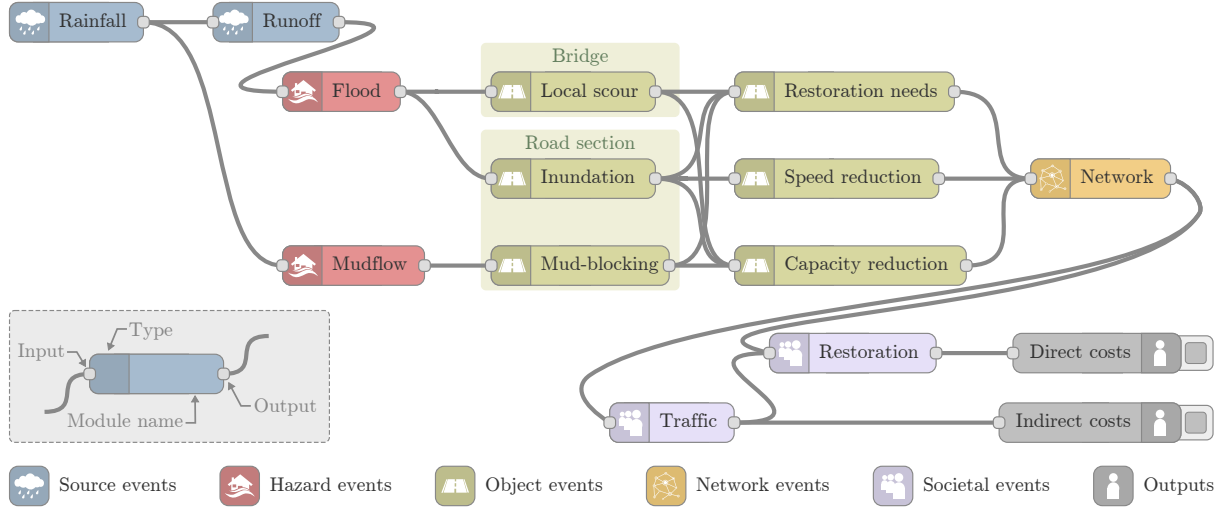
Figure 1. Schematic overview of the modules used for the application. Modules, represented by nodes with certain inputs and outputs, are related to the events that need to be modeled to estimate risk. The assessment starts with the modeling of a random *rainfall* and its corresponding *runoff*. Estimated discharge values at river stations of interest are used to simulate the *flood* propagation, including the inundation of the area. A *mudflow* can be randomly triggered during the rainfall if accumulated precipitation values exceed certain thresholds. In the next step, expected damages (i.e., *bridge local scour*, *road section inundation*, *road section mud-blocking*), functional losses (i.e., *speed reduction*, *capacity reduction*) and *restoration needs* (i.e., restoration cost, restoration time) are determined for each affected object in the network. The updated states of individual objects help define the new state of the entire *network*. The *traffic* through the network is then simulated. *Restoration* interventions are executed to enable the network to provide an adequate level of service again by changing the state of damaged objects. The costs for the restoration are accounted as *direct costs*, while the costs related to additional vehicle travel time through the network and missed trips are accounted as *indirect costs*.

Calibration : Records from precipitation measurement stations located near the study area (see Figure 2.) were used to calibrate the model. Extreme events that have been not recorded were extrapolated from the data using extreme value statistics.

Assumptions and limitations : Historical data can be used to recreate new rainfall events. In this process, values can be a certain amount up- or downscaled to produce the desired return period. The rainfall event could only occur in a period between 1 and 72 hours. This approach is limited to the recreation and modification of historical events, new, unobserved events cannot be produced, i.e., changes in the movement of the rainclouds, the spatial coverage of the clouds, ...

2.2   Runoff

Inputs :

$P_{\tau^{\mathrm{rain}}}$ – A time series of precipitation fields over period τ, where each cell values $p_{c,t} \in P_t$ with $t \in \tau^{\mathrm{rain}}$ represented the rainfall intensity per time step [mm/hour].

Outputs :

$Q_{r,t}$ – Hydrographs for different sections r of the rivers in the area of study, which were generated using the excess of cells located at the basin outlets as a function of time t in [m³/s].

Resources :

CN – Raster file with the runoff curve numbers [−] for predicting direct runoff and infiltration from rainfall excess. These numbers are related to soil type, soil infiltration capability, land use, and the depth of the seasonal high water table.

ϱ – Storage coefficient for linear reservoirs [hour].

DEM – Raster file for the digital elevation model (DEM) [m], to calculate the runoff directions.

Process : The precipitation excess was computed for each cell using the Soil Conservation Service (SCS) Curve Number (CN) model. This model estimates precipitation excess as a function of cumulative precipitation, soil cover, land use, and antecedent moisture general watershed databased on an empirical equation (Feldman, 2000):

$$p_{c,t}^e = \frac{(\mathrm{CN}_c \cdot (p_{c,t}+50.8)-5080)^2}{\mathrm{CN}_c \cdot (\mathrm{CN}_c \cdot (p_{c,t}-203.2)+20320)} \qquad (1)$$

where $p_{c,t}^e$ is the accumulated precipitation excess for cell c at time t, $p_{c,t}$ is the corresponding precipitation value, and CN_c is the curve number for the cell c.

Each cell's excess was then lagged to the basin outlet according to the cell's travel time. This translation time to the outlet was computed through a grid-based travel-

time model:

$$t_{\boldsymbol{c}}^{\mathrm{runoff}} = t^{\mathrm{runoff}} \cdot \frac{d_{\boldsymbol{c}}^{\mathrm{runoff}}}{d^{\mathrm{runoff}}} \qquad (2)$$

where $t_{\boldsymbol{c}}^{\mathrm{runoff}}$ is the lag time of travel for a cell $\boldsymbol{c}$, t^{runoff} is the time of concentration for the watershed, $d_{\boldsymbol{c}}^{\mathrm{runoff}}$ the travel distance from cell $\boldsymbol{c}$ to the watershed outlet, and d^{runoff} the travel distance for the cell that is most distant from the watershed outlet.

The individual cell outflows $f_{\boldsymbol{c},t}^{\mathrm{out}}$ were routed through a linear reservoir, to account for the effects of watershed storage. The routing was done based on Clark's original methodology:

$$f_{\boldsymbol{c},t}^{\mathrm{out}} = \frac{2 \cdot \Delta t^{Q} \cdot (f_{\boldsymbol{c},t}^{\mathrm{in}} - f_{\boldsymbol{c},t-1}^{\mathrm{out}})}{2\varrho + \Delta t^{Q}} + f_{\boldsymbol{c},t-1}^{\mathrm{out}} \qquad (3)$$

where $f_{\boldsymbol{c},t}^{\mathrm{in}}$ is the average inflow to the storage of cell $\boldsymbol{c}$ at time t composed of the accumulated precipitation excess $p_{\boldsymbol{c},t}^{e}$ and the outflows of the neighbour cells at $t-1$, ϱ is a storage coefficient for linear reservoirs (defined in time units), and Δt^{Q} is the time interval of a hydrograph Q (here set to 1 hour).

The results from each cell were combined to produce the final hydrographs for each river station r using the corresponding estimated flows $Q_{r,t}$ for all time steps t. These flows were estimated by adding the outflow values $f_{\boldsymbol{c}_r,t}^{\mathrm{out}}$ of the cells $\boldsymbol{c}_r$ located at the watershed outlet that corresponds to the river station of interest r, and the base flow $Q_{r,0}$ of that station:

$$Q_{r,t} = Q_{r,0} + \sum_{\boldsymbol{c}_r} f_{\boldsymbol{c}_r,t}^{\mathrm{out}} \qquad (4)$$

Calibration : The model was calibrated using records from past precipitation events (see above) and their resulting increase in river discharge, measured at the gauging stations located near the study area (see Figure 2.).

Assumptions and limitations : The basins can be subdivided into grid-cells, thereby, all grid-cells within a sub-basin have the same loss-rates at the beginning of each simulation. Groundwater flow is not considered. Infiltration rate will approach zero during a rainfall event of long duration, rather than constant rate as expected. The initial abstraction does not depend upon the rainfall characteristics or timing. The storage behaviour is simplified in terms of evaporation, infiltration and groundwater flow.

2.3 Flood

Inputs :

$Q_{r,t}$ – Hydrographs for different sections of the rivers in the area of study, which were generated using the excess of cells located at the basin outlets [m^3/s].

T^{flood} – Optional, the network manager could specify the desired return period of the flood event. In this case, the simulation engine produced suitable rainfall patterns, such that the resulting hydrographs led to the targeted return period.

Outputs :

$\boldsymbol{I}_t$ – A time series of inundation fields (i.e., raster file for every time step), where the cell values $i_{\boldsymbol{c},t}$ represented the floodwater depth above ground [m].

$Q_{r=b,t}$ – Hydrographs for different sections of the rivers in the area of study (out of which only those hydrographs for the river sections with the bridges of interest were selected during the analysis) [m^3/s].

Resources :

DEM – Raster file for the digital elevation model (DEM) [m], to extract the geometries and generate the inundated areas.

S – The friction slopes between river cross-sections, which are estimated using empirical laws i.e., the Manning formula.

Process : The governing equation describing the flow problem of the one-dimensional hydraulic model was derived by the energy equation for two neighbouring cross-sections, enclosing a channel reach of length $L_{i,i+1}$:

$$z_i + h_{i,t} + \frac{\gamma_i \cdot v_{i,t}^2}{2g} = z_{i+1} + h_{i+1,t} + \frac{\gamma_{i+1} \cdot v_{i+1,t}^2}{2 \cdot g} + \bar{S}_{i,i+1} \cdot L_{i,i+1} \qquad (5)$$

where z_i is the bed elevation with regard to the datum, $h_{i,t}$ is the water depth at time t, γ_i is the energy correction factor, and $v_{i,t}$ is the average flow velocity at time t, with all of these variables for a given cross-section i. Moreover, g is the gravitational acceleration, $\bar{S}_{i,i+1}$ is the average friction slope between both cross-sections, index i denotes an upstream cross-section, and index $i+1$ denotes a downstream cross-section. The friction slope can be calculated based on different empirical laws (e.g., the Manning formula). The average flow velocity $v_{i,t} = Q_{i,t}/A_{i,t}$ can be expressed as a function of the discharge $Q_{i,t} = Q_{r,t}$ and the wetted cross-sectional area $A_{i,t}$. At the same time, for a given cross-section i, this area $A_{i,t} = h_{i,t} \cdot b_i$ can be expressed as a function of the water depth $h_{i,t}$ at time t and the width of the channel b_i. Equation (5) allows to compute the water surface profiles from one cross-section to the next. For most cases, this has to be done numerically. Finally, the water depth h values at each river cross-section were interpolated to obtain an inundation field $\boldsymbol{I}_t$, representing a raster file for time t.

Calibration : Historic records from gauging stations along the rivers (see Figure 2.) were used to calibrate the

model. Extreme events that have been not recoded were extrapolated from the data using extreme value statistics. Simulation results were compared, additionally, with hazard maps from the region.

Assumptions and limitations : The flow is assumed to be unidirectional (i.e. parallel to the main channel flow). No sediment transport or debris are considered. Storage and recirculation areas are not considered. The model cannot reproduce flood events with extreme non-uniformity and spatial variability of the flow patterns.

2.4 Mudflow

Inputs :

$P_{\tau^{\text{rain}}}$ – A time series of precipitation fields (i.e., raster file for every time step) over period τ, where each cell values $p_{c,t} \in P_t$ with $t \in \tau^{\text{rain}}$ represented the rainfall intensity per time step [mm/hour].

Outputs :

L_t – A time series of mudflow fields (i.e., raster file for every time step), where the cell values $l_{c_\ell,t}$ represented the deposited mudflow volume [m^3].

Resources :

DEM – Raster file for the digital elevation model [m].

$\mathcal{L}$ – Shape file with pre-calculated potential mudflow locations and geometries, where $\ell \in \mathcal{L}$ is a certain mudflow event. Source data was taken from Losey and Wehrli (2013).

Process : Potential mudflow locations c_ℓ were obtained from Losey and Wehrli (2013). The probability that a mudflow could occur was estimated based on precipitation thresholds obtained by using the empirical intensity-duration function for sub-alpine regions proposed by Zimmermann et al. (1997):

$$p_{c_\ell,\tau}^{\text{mudflow}} = 32 \cdot \tau_{c_\ell,t}^{-0.72} \tag{6}$$

where $p_{c_\ell,\tau}^{\text{mudflow}}$ is the precipitation threshold in mm/hour and $\tau_{c_\ell,t}$ is the duration of the rainfall event until time t at the potential mudflow location c_ℓ. For each potential mudflow location, the respective precipitation values $p_{c_\ell,t}$ were extracted from the rainfall model and used as points of comparisons. If the threshold was exceeded ($\sum_{t \in \tau_{c_\ell,t}} p_{c_\ell,t} > p_{c_\ell,\tau}^{\text{mudflow}}$) at a given time step, a probability of being triggered was assigned to the event, based on the slope factor of safety (FS) (Skempton and Delory, 1952):

$$\text{FS}_{\ell,t} = \frac{(c^s + c^r) + (\gamma^s - m^t \cdot \gamma^w) \cdot z^s \cdot \cos^2 S \cdot \tan\phi}{\gamma^s \cdot z^s \cdot \sin S \cdot \cos S} \tag{7}$$

where c^s and c^r are the cohesion of soil and roots respectively, γ^s is the specific weight of soil, $m^t = z_t^w / z^s$

is the fraction between water table depth z_t^w at time t and the soil depth z^s, γ^w is the specific weight of water, S is the slope angle, and ϕ is the angle of internal friction. The water table depth z_t^w is composed of the initial water table depth z_0^w and the additional depth $\sum_{t \in \tau_{c_\ell,t}} p_{c_\ell,t}$. All values can be assumed to correspond to the potential mudflow location c_ℓ. Based on probabilistic input parameters (Table 1), a Monte Carlo scheme was used to generate $j = 100,000$ FS values. This data set was then used to derive the triggering probability ($\mathbb{P}[\ell|t] = \frac{1}{j} \sum_j \mathbb{1}_{FS_{\ell,t} < 1}$).

Table 1. Probabilistic inputs for mudflow triggering.

Sym.	Description	Distr.	Values	Unit
c^s	cohesion of soil	Norm	5.04, 2.18	kPa
c^r	cohesion of roots	Norm	3.41, 2.36	kPa
γ^s	specific weight of soil	Unif	18, 33	kN/m^3
γ^w	specific weight of water	Det	9.81	kN/m^3
z^s	soil depth	Unif	0.1, 1.5	m
S	slope angle	Unif	35, 65	Deg
ϕ	angle of internal friction	Norm	30, 5	Deg

The volume V_ℓ of each mudflow was estimated by taking into account the runout length R_ℓ of the fan using an empirical relation proposed by Rickenmann (1999):

$$V_\ell = \left(\frac{R_\ell}{15}\right)^2 \tag{8}$$

The increase in elevation per cell was calculated by dividing the volume by the area of the fan. The output of the model was a time series of raster files L_t, whose cell values corresponded to the additional elevation caused by the mudflows.

Calibration : Historical records of rainfall intensity and triggered mudflows were used to calibrate the triggering probability of these events. The pre-calculated mudflow locations and geometries were compared with observations from different test areas and qualitative evaluated by experts (see Losey and Wehrli (2013)).

Assumptions and limitations : Intensity-duration function and a probabilistic infinite slop model can describe the triggering of mudflows. This approach is limited to the recreation and modification of predefined potential mudflow locations and geometries, "new" – unobserved – events cannot be produced.

2.5 Object fragility

2.5.1 Bridge local scour

Inputs :

$Q_{r=b,t}$ – Hydrographs for different sections of the rivers in the area of study (out of which only those hydrographs for the river sections r with the bridges

of interest b were selected during the analysis) [m^3/s].

Outputs :
  DS$^{\mathrm{scour}}$ – Time series of damage state exceedance probabilities considering cumulative damages for bridges due to local scour.

Resources :

  DEM – Raster file for the digital elevation model (DEM) [m], to extract the river geometries.

  e – Objects with associated properties such as type of bridge and number of piers.

Process : Empirical relationships from Arneson et al. (2012) were used to quantify the excavated depth $h_{e,r,t}^{\mathrm{scour}}$ of an object e located near river station r due to local scour at time t:

$$ h_{e,r,t}^{\mathrm{scour}} = 2.0 \cdot \kappa_1 \cdot \kappa_2 \cdot \kappa_3 \cdot h_r \cdot \left(\frac{a_e}{h_{r,t}} \right)^{0.65} \left(\frac{v_{r,t}}{\sqrt{g \cdot h_{r,t}}} \right)^{0.43} \tag{9} $$

where the κ parameters are corrective coefficients and a_e represents the pier width. The relationship between the water depth $h_{r,t}$, flow velocity $v_{r,t}$ and discharge $Q_{r,t}$ is given in Section 2.3. Based on probabilistic input parameters (Table 2), a Monte Carlo scheme was implemented to generate 100,000 scour depths $h_{e,r,t}^{\mathrm{scour}}$ and to analyse the probability of failure ($\mathbb{P} = \frac{1}{j} \sum_j \mathbb{1}_{h_{e,r,t}^{\mathrm{scour}} > h_{\max}^{\mathrm{scour}}}$).

Table 2. Probabilistic inputs for bridge local scour.

Sym.	Description	Distr.	Values	Unit
κ_1	factor for pier shape	Det	1	–
κ_2	factor for angle of attack	Norm	1.23, 0.16	–
κ_3	factor for bed from	Norm	1.1, 0.055	–
a^e	pier width	Unif	0.8, 0.85	m
$h_{\max}^{\mathrm{scour}}$	critical scour depth	Norm	5.7, 1.12	m

This dataset was then entered into a maximum likelihood estimation function to generate fragility functions for the four damage states given in Table 1 with respect to flow discharge $Q_{r=b,t}$. The functions followed log-normal relationships:

$$ \mathbb{P}[\mathrm{DS} \geq s_i | Q_{r=b,t}] = \Phi \left(\frac{\ln Q_{r=b,t} - \mu}{\sigma} \right) \tag{10} $$

where DS represents the realization of the damage state to be compared against a threshold damage state s_i with $i \in [0, 1, 2, 3]$, and $Q_{r=b,t}$ represents the hazard intensity measure at river station r next to bridge b at time t. The derived fragility parameters for the scour damage states are given in Table 2.

Assumptions and limitations : Only local pier scour is assumed while scour at the embankments is neglected. The scour process is only determined by the discharge values (i.e. flow properties of the section), sediment transport is not (directly) considered in the scour depth calculation.

2.5.2 Road section inundation

Inputs :
  I_t – A time series of inundation fields, where each cell value $i_{c,t}$ represented the floodwater depth above ground [m].

Outputs :
  DS$^{\mathrm{inun}}$ – Time series of damage state exceedance probabilities considering cumulative damages for road sections/subsections due to inundation.

Resources :

  n – Subsections of the objects with associated properties such as the road type.

Process : The fragility functions were constructed assuming that (i) the general width of high-speed (major) roads was $12\,\mathrm{m}$ and that of local (minor) roads was $6\,\mathrm{m}$, (ii) all pavements had a sub-base, with major roads having a sub-base twice as thick as that of minor roads, (iii) major road layers were considered to always be thicker than local road layers, (iv) one day of inundation could compromise the performance of the sub-grade layer (Roslan et al., 2015), and (v) any amount of traffic on a road section with a compromised sub-grade layer would result in reconstruction. Log-normal fragility functions were fitted based on three additional assumptions:

  – the sub-base of a linear meter of major road section can store $0.35\,\mathrm{m}^3$ of water (Walsh, 2011), leading to assume that inundation depths below $2.92\,\mathrm{cm}$ caused problems to major road sections with 5 % probability (the same threshold for minor road sections was set to $1.46\,\mathrm{cm}$),

  – an inundation depth of $30\,\mathrm{cm}$ is the average depth at which passenger cars start to float, which implies that objects as heavy as passenger cars can be transported throughout the road network, leading to assume the collapse of the drainage function and significant damages to various road elements in addition to making the subgrade vulnerable with 95 percent probability,

  – the median inundation depth values of the fragility functions arbitrarily increase by $5\,\mathrm{cm}$ as the damage states increase, with median values of major roads higher by $10\,\mathrm{cm}$ than those of local roads to illustrate that pavement thickness is a vulnerability factor as indicated by Zhang et al. (2008) and ac-

knowledge that major roads undergo a more rigorous design process than local roads.

Table 2 shows the parameters of the fragility function when inundation depth was used as an intensity measure. Such depth was associated with the need to clean up a given road section, damages to selected elements, and the eventual loss of the subgrade.

Assumptions and limitations : Other modes of failure, in particular, the blockage of drainage, delamination, erosion and washed out elements were associated with runoff flow. Although important to model, these phenomena were not included in the model, but should certainly be considered in the future.

2.5.3 Road section mud-blocking

Inputs :
L_t – A time series of raster files, each of which contained cell $l_{c_\ell,t}$ values corresponding to the deposited debris volumes of a mudflow [m^3].

Outputs :
$\mathbf{DS}^{\mathrm{block}}$ – Time series of damage state exceedance probabilities considering cumulative damages for road sections/subsections due to mud-blocking.

Resources :

n – Subsections of the objects with associated properties such as the road type.

Process : As part of a survey conducted by Winter et al. (2013), experts assigned damage state exceedance probabilities to debris flow volumes for specific damage states and road categories (i.e., major roads and minor roads). Volumes were understood to intersect a road section of $500\,\mathrm{m}$. Experts also provided a score representing their level of expertise.

This dataset was used to derive fragility functions for pavement mud-blocking. For every combination of damage state and road category, four expert responses were randomly sampled from the survey dataset. This process resulted in different scenarios of relationships between debris flow volumes and damage state exceedance probabilities. These sampled relationships, along with the recorded expertise level scores, were entered into a maximum likelihood estimation function to generate the fragility functions given in Table 1.

Assumptions and limitations : It was assumed that the results of the survey by Winter et al. (2013), focused on debris flow, could be used for determining a relationship between mudflows and road sections.

2.6 Object functionality

2.6.1 Capacity reduction

Inputs :

$\mathbf{DS}^{\mathrm{scour}}$ – Time series of damage state exceedance probabilities considering cumulative damages for bridges due to local scour.

$\mathbf{DS}^{\mathrm{inun}}$ – Time series of damage state exceedance probabilities considering cumulative damages for road sections/subsections due to inundation.

$\mathbf{DS}^{\mathrm{block}}$ – Time series of damage state exceedance probabilities considering cumulative damages for road sections/subsections due to mud-blocking.

Outputs :
$\langle\lambda\rangle_{n,t}$ – Time series of expected capacity reduction for bridges with scoured piers, inundated road sections/subsections and mud-blocked road sections/subsections.

Resources :

n – Subsections of the objects with associated properties such the road type.

Process : The expected capacity reductions were determined as functions of time-dependent damage state exceedance probabilities $\mathbf{DS}$ and functional loss values λ associated with the investigated damage states s_i ($i \in [0,1,2,3]$) (see Table 3):

$$\langle\lambda\rangle_{n,t} = \sum_{i=0}^{3} \lambda_{s_i} \cdot \mathbf{DS}_{s_i,t} \tag{11}$$

where $\langle\lambda\rangle \in [0,1]$ is the expected capacity reduction of a specific subsection n at a specific time t in the simulation.

Assumptions and limitations : The estimated loss values λ where obtained from a survey conducted by D'Ayala and Gehl (2015). The most conservative values were selected whenever possible. For bridge local scour, the survey had a range of answers for a general bridge local scour category, which did not necessarily match with the proposed damage limit state functions of this work.

2.6.2 Speed reduction

Inputs :
I_t – A time series of inundation fields, where each cell value $i_{c,t}$ represented the floodwater depth above ground [m].

Outputs :
$\langle\phi\rangle_{n,t}$ – A time series of speed reduction for inundated road sections/subsections.

Resources :

n – Subsections of the objects with associated properties such as maximum allowed speed.

Process : During the hazard event period, the relationship between inundation depths and feasible speed of vehicles on the road was derived from the data presented by Pregnolato et al. (2017). An exponential function was

fitted to these data to describe the limit vehicle speed in a road as a function of inundation depth.

$$v_{n,t}(i_{\boldsymbol{c}_n,t}) = \begin{cases} v^{\max} \cdot \exp\{-0.10814 \cdot i_{\boldsymbol{c}_n,t}\} & \text{for} \quad i_{\boldsymbol{c}_n,t} \leq 30\,\text{cm} \\ 0 & \text{otherwise} \end{cases}$$

(12)

where $v_{n,t}$ is the maximum acceptable velocity that ensures safe control of a vehicle through subsection n at time t when considering the inundation depth $i_{\boldsymbol{c}_n,t}$, and $v^{\max}$ is the maximum allowed speed on any road. The functional loss due to speed reduction for a section n at time t, was determined by:

$$\langle \phi \rangle_{n,t} = \frac{\max(0, v_n^{\max} - v_{n,t}(i_{\boldsymbol{c}_n,t}))}{v_n^{\max}}$$

(13)

where $\langle \phi \rangle \in [0,1]$ is the expected speed reduction at a specific subsection n at time t in the simulation and $v_n^{\max}$ is the maximum allowed speed on subsection n.

Assumptions and limitations : The maximum allowed speed $v^{\max}$ in Equation (12) was set to be $120\,\text{km/h}$. No distinction is made between different types of vehicles (e.g., cars, trucks, etc.).

2.7 Object restoration needs

Inputs :

$\mathbf{DS}^{\text{scour}}$ – Time series of damage state exceedance probabilities considering cumulative damages for bridges due to local scour.

$\mathbf{DS}^{\text{inun}}$ – Time series of damage state exceedance probabilities considering cumulative damages for road sections/subsections due to inundation.

$\mathbf{DS}^{\text{block}}$ – Time series of damage state exceedance probabilities considering cumulative damages for road sections/subsections due to mud-blocking.

Outputs :

$\langle \bar{\lambda} \rangle_{n,t}$ – Time series of the expected capacity reduction during restoration intervention for bridges with scoured piers, inundated road sections/subsections and mud-blocked road sections/subsections.

$\langle c \rangle_{n,t}$ – Time series of the expected restoration costs [CHF] for bridges with scoured piers, inundated road sections/subsections and mud-blocked road sections/subsections.

$\langle \tau \rangle_{n,t}$ – Time series of the expected restoration times [hours] for bridges with scoured piers, inundated road sections/subsections and mud-blocked road sections/subsections.

Resources :

$\mathcal{C}^{\text{dc}}$ – Set of direct cost parameters including fixed costs c^{fix} and variable costs c^{var} for the restoration of bridge local scour, road section inundation and road section mud-blocking (see Table 4.).

Process : For each section n in a damage state s_i ($i \in [0,1,2,3]$), a restoration intervention was assigned. Associated with each intervention were (i) the capacity losses due to the execution of the intervention $\bar{\lambda}_n$, (ii) the length of time required to execute the intervention $\tau_n \geq 0$, and (iii) the cost of the intervention $c_n \geq 0$. This cost was composed of a fixed part c_n^{fix} (e.g., site setup) and a variable part c_n^{var} (e.g., CHF/m^2 of pavement, CHF/m^3 of concrete). Based on the derived time series of damage state exceedance probabilities $\mathbf{DS}$, expected capacity reduction during restoration $\langle \bar{\lambda} \rangle_{n,t}$, the expected restoration costs $\langle c \rangle_{n,t}$ and durations $\langle \tau \rangle_{n,t}$ for each section were calculated.

$$\langle \bar{\lambda} \rangle_{n,t} = \sum_i^3 \bar{\lambda}_{n,s_i} \cdot \mathbf{DS}_{s_i,t}$$

(14)

$$\langle c \rangle_{n,t} = \sum_i^3 \left(c_{n,s_i}^{\text{fix}} + c_{n,s_i}^{\text{var}} \right) \cdot \mathbf{DS}_{s_i,t}$$

(15)

$$\langle \tau \rangle_{n,t} = \sum_i^3 \tau_{n,s_i} \cdot \mathbf{DS}_{s_i,t}$$

(16)

Assumptions and limitations : Although multiple restoration strategies might be possible, (e.g., putting more effort into the restoration of critical objects) it was assumed that only one strategy with expected costs and restoration time is implemented.

2.8 Network

Inputs :

$\langle \lambda \rangle_{n,t}$ – Time series of expected capacity reduction for bridges with scoured piers, inundated road sections/subsections and mud-blocked road sections/subsections.

$\langle \phi \rangle_{n,t}$ – A time series of speed reduction for inundated road sections/subsections.

$\langle \bar{\lambda} \rangle_{n,t}$ – A time series of the expected capacity reduction during restoration intervention

$\langle c \rangle_{n,t}$ – A time series of the expected restoration costs [CHF].

$\langle \tau \rangle_{n,t}$ – A time series of the expected restoration times [hours] for bridges with scoured piers, inundated road sections/subsections and mud-blocked road sections/subsections.

$\boldsymbol{R}_t$ – A restoration program, defining when each damaged object is to be restored.

Outputs :

$\boldsymbol{G}$ – A time series of routable network graphs that can be used for traffic assignment.

$\langle \lambda \rangle_{e,t}$ – A time series of the expected aggregated capacity reduction for object e.

$\langle \phi \rangle_{e,t}$ – A time series of the expected aggregated speed reduction for object e.

Process : The road network was modelled as a graph $G = (\mathcal{V}, \mathcal{E})$ composed of 1,520 vertices (i.e., 37 centroids, 1,056 junctions, and 427 changes in road geometric features) and 3,202 directed edges $e \in \mathcal{E}$, also referred to as links or objects.

An aggregation routine of subsections' functional losses was implemented, which computed the expected functional loss at an edge level by identifying the maximum expected functional loss of the subsections that are part of the edge. The functional loss related to road capacity reduction for an edge e at time t, was determined by:

$$\langle\lambda\rangle_{e,t} = \max_{n \in e}(\langle\lambda\rangle_{n,t}) \tag{17}$$

where $\langle\lambda\rangle_{e,t}$ is the expected aggregated capacity reduction for object e at time t and $\langle\lambda\rangle_{n,t}$ is the expected capacity reduction of a specific subsection $n \in e$. At the same time, the functional loss due to speed reduction for an edge e at time t, was determined by:

$$\langle\phi\rangle_{e,t} = \max_{n \in e}(\langle\phi\rangle_{n,t}) \tag{18}$$

where $\langle\phi\rangle_{e,t}$ is the expected aggregated speed reduction for object e at time t and $\langle\phi\rangle_{n,t}$ is the expected speed reduction for a specific subsection $n \in e$.

Assumptions and limitations : The worst section of the object determines the whole object behaviour, i.e. a weakest link approach.

2.9 Traffic

Inputs :

G – A time series of routable network graphs that can be used for traffic assignment.

$\langle\lambda\rangle_{e,t}$ – A time series of the expected aggregated capacity reduction for object e.

$\langle\phi\rangle_{e,t}$ – A time series of the expected aggregated speed reduction for object e.

Outputs :

$x_{e,t}$ – A time series of traffic flow for each edge e in the network.

$t_{e,t}^{\text{traffic}}$ – A time series of travel time for each edge e in the network.

$\mathcal{P}_{od,t}^0$ – A time series of od-paths where no flow is possible (missed trips).

Resources :

od – An origin-destination matrix of the area.

Process : The traffic flow $x_{e,t}$ for edge e at time t was estimated by solving the user equilibrium assignment, Equation (19a) subjected to Equations. (19b) and (19c).

$$x_{e,t} \in \min \sum_e \int_0^{x_{e,t}} C^{\text{traffic}}(\omega)\, d\omega \tag{19a}$$

subjected to

$$\sum_{P \in \mathcal{P}_{od,t}^1} f_{od}(P) = d_{od} \qquad \forall od \tag{19b}$$

$$f_{od}(P) \geq 0 \qquad \forall P \in \mathcal{P}_{od,t}^1, \forall od \tag{19c}$$

where

$$x_{e,t} = \sum_{od} \sum_{e \in P \in \mathcal{P}_{od,t}^1} f_{od}(P) \tag{19d}$$

where $f_{od}(P)$ is the function to estimate the flow between origin o and destination d on path P. While $\mathcal{P}_{od,t}^1$ refers to the set of od-paths where some flow is still possible, $\mathcal{P}_{od,t}^0$ refers to the set of od-paths where no flow is possible. The demand constraints Equation (19b) state that the flow on a given od-pair has to equal the demand $d_{od} \geq 0$, for all od. The non-negativity constraints Equation (19c) are required to ensure that the solution of the program will be physically meaningful.

In terms of the edge cost function C^{traffic}, which estimates the travel time $t_{e,t}^{\text{traffic}}$ through edge e at time t when using the corresponding traffic flow as an input, has been defined using the formulation proposed by the Bureau of Public Roads (1964):

$$C^{\text{traffic}}(x_{e,t}) := (1 - \langle\phi\rangle_{e,t}) \cdot t_{e,0}^{\text{traffic}} \left(1 + \alpha_e \left(\frac{x_{e,t}}{(1 - \langle\lambda\rangle_{e,t}) \cdot y_{e,0}} \right)^{\beta_e} \right) \tag{20}$$

where $t_{e,0}^{\text{traffic}}$ is the initial free flow travel time, $y_{e,0}$ the initial edge capacity, $\langle\phi\rangle_{e,t}$ the expected speed reduction, $\langle\lambda\rangle_{e,t}$ the expected capacity reduction, and α_e and β_e are parameters for calibration, with typical values $\alpha = 0.15$ and $\beta = 4$.

Calibration : Data from traffic count stations in the study area were used to calibrate the initial traffic assignment, (i.e., before the hazard events occurred).

Assumptions and limitations : A static user equilibrium traffic assignment model, based on the BPR functions to emulate the traffic flow conditions are implemented. Although this model is mathematical rather simple, computationally inexpensive and widely used in literature, it has some limitations when it comes to a realistic representation of traffic flow, e.g., it is assumed that travellers have full knowledge of the traffic conditions, which is clearly not the case. It also does not account for changes in the travel pattern after a disruptive event, although studies show this behaviour is considerably different from before a disruptive event.

2.10 Restoration

Inputs :

$\langle\bar{\lambda}\rangle_e$ – Time series of the expected capacity reduction during restoration intervention

$\langle \tau \rangle_e$ – Time series of the expected restoration times [hours] for bridges with scoured piers, inundated road sections and mud-blocked road sections.

$\mathcal{P}^0_{od,t}$ – A time series of od-paths where no flow is possible.

Outputs :

$\boldsymbol{R}_t$ – A restoration program, defining when (t), each damaged object (e) is restored and the assigned work crew to the task.

Resources :

$x_{e,t=0}$ – The initial traffic flow on the network.

Process :

1. All edges with functional capacity losses greater than 10% were labelled as "objects in need of restoration".

2. All objects with a need of restoration were ranked according some prioritization criteria. First, edges which disconnect parts of the network ($e \in \mathcal{P}^0_{od}$) were restored, afterwards edges with an initial high traffic flow $x_{e,t=0}$ were prioritized.

3. The expected durations $\langle \tau \rangle$ for the objects were assigned.

4. The available work crews were assigned to the top ranked objects. The capacity of the objects under restoration was set to $\langle \bar{\lambda} \rangle$.

5. After the period $\langle \tau \rangle$ the object was restored and removed from the list.

6. The work crew was assigned to the next object (step 4).

Assumptions and limitations : Objects are restored only if the capacity loss is greater than 10% otherwise, it is assumed that the objects are restored during their normal maintenance process. Only one work crew can repair an object, i.e. multiple work crews working on the same object is not supported.

2.11 Direct and indirect costs

2.11.1 Direct costs

Inputs :

$\langle c \rangle_{n,t}$ – A time series of the expected restoration costs [CHF] for bridges with scoured piers, inundated road sections and mud-blocked road sections.

Outputs :

C^{dc} – The expected direct costs for restoring the physical damages of the considered objects.

Process : Only restoration costs were considered as direct costs. The overall expected direct costs C^{dc} was the sum of the expected direct costs for each intervention executed. It was assumed that the selected restoration program does not affect intervention costs.

$$C^{\mathrm{dc}} = \sum_n \max_t(\langle c \rangle_{n,t}) \tag{21}$$

Cost estimates were based on Staubli and Hirt (2005) and from a survey conducted by D'Ayala and Gehl (2015). For each object type and damage state, a restoration strategy was derived, and for each strategy, cost and duration values were approximated (Table 4).

Assumptions and limitations : Costs taken from the literature are adjusted to 2017 price levels. To avoid over interpreting the specific values that were in the example, monetary units are used instead of real currency. Variable costs are only dependent on the length of the object.

2.11.2 Indirect costs

Inputs :

$\mathcal{P}^0_{od,t}$ – A time series of od-paths where no flow is possible (missed trips).

$x_{e,t}$ – A time series of traffic flow for each edge e in the network.

$t^{\mathrm{traffic}}_{e,t}$ – A time series of travel time for each edge e in the network.

Outputs :

C^{ic} – The expected indirect costs for prolongation and missed trips.

Resources :

$\mathcal{C}^{\mathrm{ic}}$ – Set of indirect cost parameters including: value of travel time (ξ), mean fuel price (ζ), operating costs without fuel (ρ), and value of a missed trip (ϵ).

Process : The indirect costs were comprised of costs for the temporal prolongation of travel and costs due to a loss of connectivity. The overall indirect costs C^{ic} were measured as the difference between indirect costs at time t and the indirect costs at time 0 when the network was fully functional.

$$C^{\mathrm{ic}} = \sum_t \left[\sum_{e \in \mathcal{P}^1_{od,t}} C^{\mathrm{ic,pt}}(x_{e,t}) + C^{\mathrm{ic,lc}}(\mathcal{P}^0_{od,t}) \right] \tag{22}$$

where $C^{\mathrm{ic,pt}}$ was a cost function dependent on the edge traffic flow $x_{e,t}$ in time t through edge e that was part of the set of feasible paths $\mathcal{P}^1_{od,t}$ identified in time t, and $C^{\mathrm{ic,lc}}$ was a cost function dependent on a loss of connectivity, which was determined based on the set of unfeasible paths $\mathcal{P}^0_{od,t}$ identified in time t.

Temporal prolongation of travel – The cost function attributed to traffic flow included sub-functions to estimate the costs related to travel time $C^{ic,\mathrm{tt}}$ and vehicle operation $C^{ic,\mathrm{vo}}$.

$$C^{ic,\mathrm{pt}}(x_{e,t}) = C^{ic,\mathrm{tt}}(x_{e,t}) + C^{ic,\mathrm{vo}}(x_{e,t}) \tag{23}$$

Travel time costs were estimated based on the increased amount of time people spent travelling, which was linked directly to the flow on an edge.

$$C^{\text{ic,tt}}(x_{e,t}) = (t^{\text{traffic}}_{e,t} \cdot x_{e,t} - t^{\text{traffic}}_{e,0} \cdot x_{e,0}) \cdot \xi \qquad (24)$$

where $t^{\text{traffic}}_{e,t}$ was the travel time on edge e at time t in hours and ξ was the value of travel time. Based on the work of the Swiss Association of Road and Transport Experts (VSS, 2009a), ξ was assumed to be 23.02 CHF/hour per vehicle.

Vehicle operation costs were incurred as a result of fuel consumption and vehicle maintenance.

$$C^{\text{ic,vo}}(x_{e,t}) = (x_{e,t} - x_{e,0}) \cdot l_e \cdot (\zeta \cdot F + \rho) \qquad (25)$$

where l_e was the length of edge e, ζ was the mean fuel price (1.88 CHF/litres), F was the mean fuel consumption (6.7 litres per 100 km per vehicle), and ρ was the operating cost without fuel (14.39 CHF/$(100 \cdot \text{veh} - \text{km})$) (VSS, 2009b).

Loss of connectivity – The costs due to a loss of connectivity were estimated based on the unsatisfied demand per time t and the resulting costs due to a loss caused of the missed trips.

$$C^{\text{ic,lc}}(\mathcal{P}^0_{od,t}) = \sum_{od} \sum_{P \in \mathcal{P}^0_{od,t}} f_{od}(P) \cdot \epsilon \qquad (26)$$

where f_{od} was a function used to estimate the demand on any given path for a specific origin-destination od, and ϵ was the monetary loss due to missed trips (i.e., cost of lost labour productivity per hour), which was assumed to be 83.27 CHF for every time step of simulation during the hazards event period. The missed trip cost during the restoration period was assumed to be 666.16 CHF for every simulation time step.

Assumptions and limitations : Business interruptions and other indirect costs are not considered.

3   Nomenclature

General

c	raster cell
DEM	digital elevation model
r	river station
t	time step
τ	duration

Subscripts

b	river station next to bridge b
c	variable or function associated with raster cell c
e	variable or function associated with the object e
i	running variable e.g. index of a river cross section
ℓ	variable or function associated with mudflow ℓ
n	variable or function associated with the subsection n
r	variable or function associated with river station r
t	variable or function at time step t

Superscripts

dc	variable or function associated with the direct costs
flood	variable or function associated with the flood model
ic	variable or function associated with the indirect costs
inun	variable or function associated with the pavement inundation model
block	variable or function associated with the pavement mud-blocking model
block	variable or function associated with the pavement mudblocking model
in	inflow
out	outflow
rain	variable or function associated with the rainfall model
mudflow	variable or function associated with the mudflow model
runoff	variable or function associated with the runoff model
scour	variable or function associated with the pier-scour model

Rainfall

$\boldsymbol{P}_{\tau^{\text{rain}}}$	precipitation fields over a period τ^{rain}
$\mathcal{P}^{\text{rain}}$	catalogue of historic precipitation fields over time
$p_{c,t}$	precipitation intensity at cell c for time t
T^{rain}	return period
τ^{rain}	duration of the rainfall event

Runoff

CN	runoff curve number
Δt^Q	time interval of a hydrograph Q
d^{runoff}	travel distance from the cell that is most distant to the watershed outlet
d^{runoff}_c	travel distance from cell c to the watershed outlet
$f^{\text{in}}_{c,t}$	average inflow for cell c at time t
$f^{\text{out}}_{c,t}$	outflow of cell c at time t
$Q_{r,0}$	base flow for a river station r
$Q_{r,t}$	hydrograph for river station r as function of t
ϱ	storage coefficient for linear reservoirs
τ^{runoff}	duration of the runoff event

t^{runoff} time of concentration for the watershed

$t_{\boldsymbol{c}}^{\mathrm{runoff}}$ lag time of travel for cell $\boldsymbol{c}$

Flood

$A_{i,t}$ wetted cross-sectional area at cross-section i at time t

b_i channel width at cross-section i

γ_i energy correction factor at cross-section i

$h_{i,t}$ water depth at cross-section i at time t

$\boldsymbol{I}_t$ inundation field at time t

$i_{\boldsymbol{c},t}$ inundation depth of cell $\boldsymbol{c}$ field at time t

$L_{i,i+1}$ channel reach length between cross-section i and cross-section $i+1$

$\bar{S}_{i,i+1}$ average friction slope between cross-section i and cross-section $i+1$

T^{flood} return period

$v_{i,t}$ average flow velocity at cross-section i at time t

z_i bed elevation with regard to the datum at cross-section i

Mudflow

c^r cohesion of roots

c^s cohesion of soil

c^{s+r} cohesion of soil and roots

$\mathrm{FS}_{\ell,t}$ factor of safety for mudflow ℓ at time t

γ^s specific weight of soil

γ^w specific weight of water

$\mathcal{L}$ set of potential mudflow locations and geometries

ℓ mudflow event

$\boldsymbol{L}_t$ mudflow elevation field at time t

m_t fraction between water table depth and the soil depth at time t

$p_{\boldsymbol{c}_\ell,\tau}^{\mathrm{mudflow}}$ precipitation threshold for intensity-duration function at cell $\boldsymbol{c}_\ell$ and time t

ϕ angle of internal friction

R_ℓ runout length of mudflow ℓ

S slope angle

$\tau_{\boldsymbol{c}_\ell,t}$ duration of the rainfall event until time t at cell $\boldsymbol{c}_\ell$

V_ℓ volume of mudflow ℓ

z^s soil depth

z_t^w water table depth at time t

Object

a_e pier width for the object e

DS   realization of a damage state

DS   time series of damage state exceedance probabilities

e object

$h_{e,r,t}^{\mathrm{scour}}$ scour depth at time t for object e located near river station r

κ corrective coefficients

λ capacity reduction value

$\langle\lambda\rangle_{n,t}$ expected capacity reduction for subsection n at time t

n subsection of an object

$\langle\phi\rangle_{n,t}$ expected speed reduction for subsection n at time t

ϕ speed reduction value

s (damage limit) state of an object

$v_{n,t}$ maximum acceptable velocity that ensures safe control of a vehicle through subsection n at time t

v^{max} maximum allowed speed

Ξ intensity measure

Network

$\mathcal{E}$ set of edges in the network graph

G routable network graph

$\langle\lambda\rangle_{e,t}$ expected aggregated capacity reduction for object e at time t

l_e length of edge

$\langle\phi\rangle_{e,t}$ expected aggregated speed reduction for object e at time t

$\mathcal{V}$ set of vertices in the network graph

Restoration

$\langle\bar{\lambda}\rangle_{n,t}$ expected capacity reduction during restoration for subsection n at time t

$\boldsymbol{R}_t$ restoration program

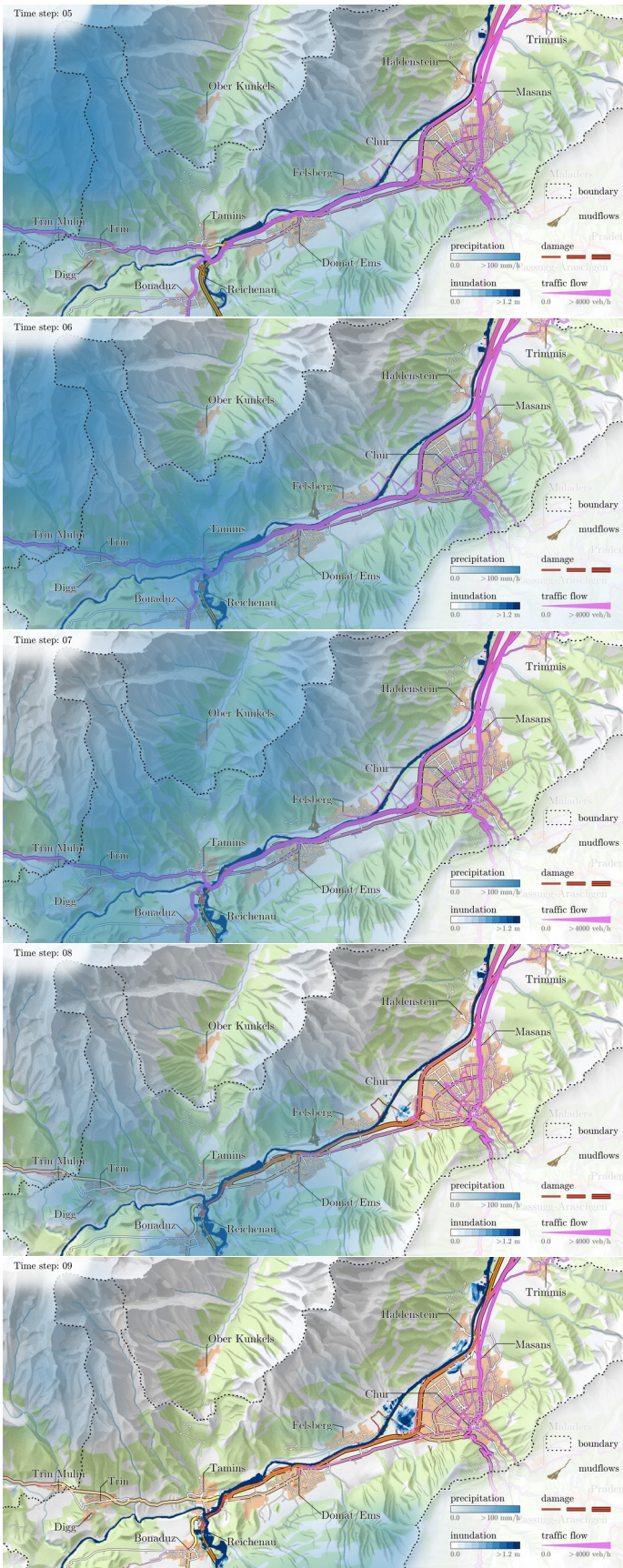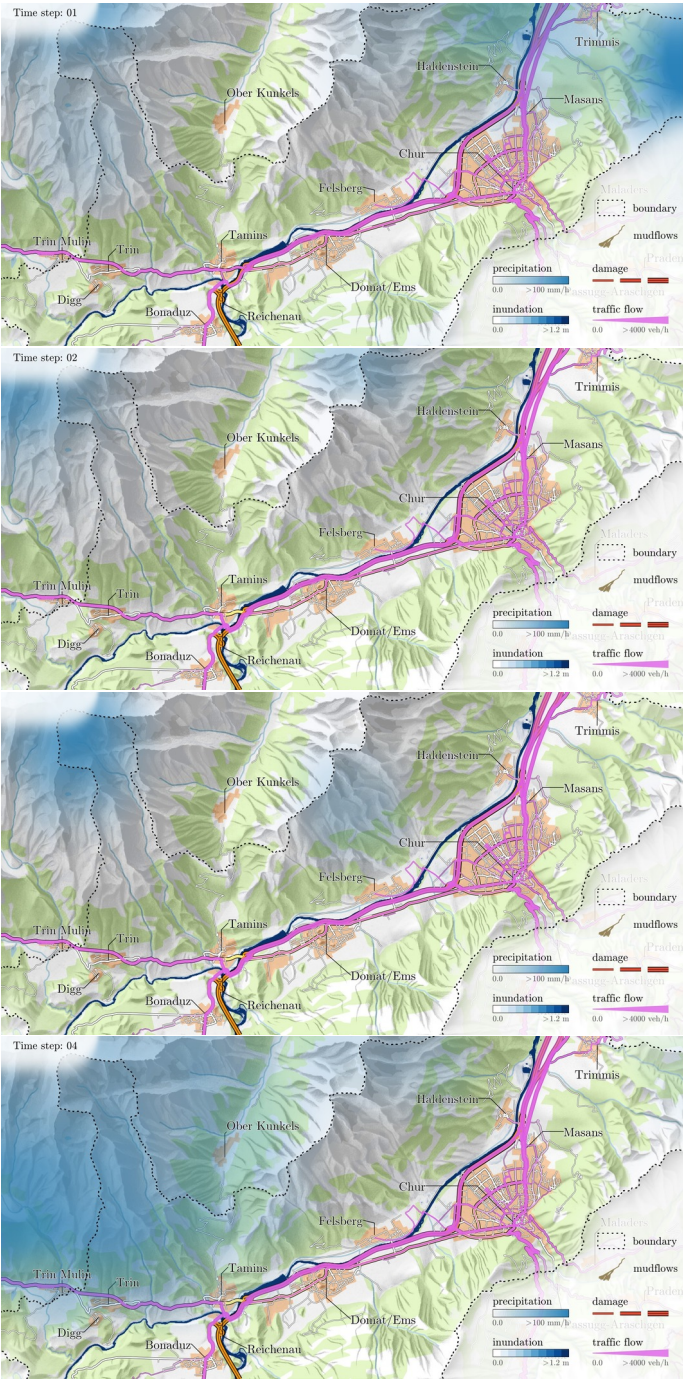$\langle\tau\rangle_{n,t}$ expected restoration time for subsection n at time t

Traffic

α_e, β_e calibration parameters for the traffic through edge e

C^{traffic} function to estimate travel cost

$f_{od}(P)$ function to estimate traffic flow on path P that connects origin-destination od

od origin-destination

P a path

$\mathcal{P}_{od,t}^0$ set of unfeasible paths at time t

$\mathcal{P}_{od,t}^1$ set of feasible paths at time t

$t_{e,t}^{\mathrm{traffic}}$ travel time through edge e in time t

$t_{e,0}^{\mathrm{traffic}}$ initial free flow travel time

$x_{e,t}$ traffic flow through edge e at time t

$y_{e,0}$ initial edge capacity

Costs

$\mathcal{C}$ set of cost parameters

$\mathcal{C}$ set of cost parameters

$\langle c\rangle_{n,t}$ expected costs of the intervention for subsection n at time t

C cost function

c_n^{fix} fixed intervention costs for subsection n

$C^{\mathrm{ic,lc}}$ function for costs due to a loss in connectivity

$C^{\mathrm{ic,pt}}$ function for costs of temporal prolongation of travel

$C^{\mathrm{ic,tt}}$ function for costs of travel time

c_n^{var} variable intervention costs for subsection n

$C^{\mathrm{ic,vo}}$ function for costs of vehicle operation

ϵ value of a missed trip

F mean fuel consumption

ρ operating costs without fuel

ξ value of travel time

ζ mean fuel price

4 System evolution

Time step: 10 / Time step: 11 / Time step: 12 / Time step: 13 / Time step: 14 / Time step: 15 / Time step: 16 / Time step: 17 / Time step: 18
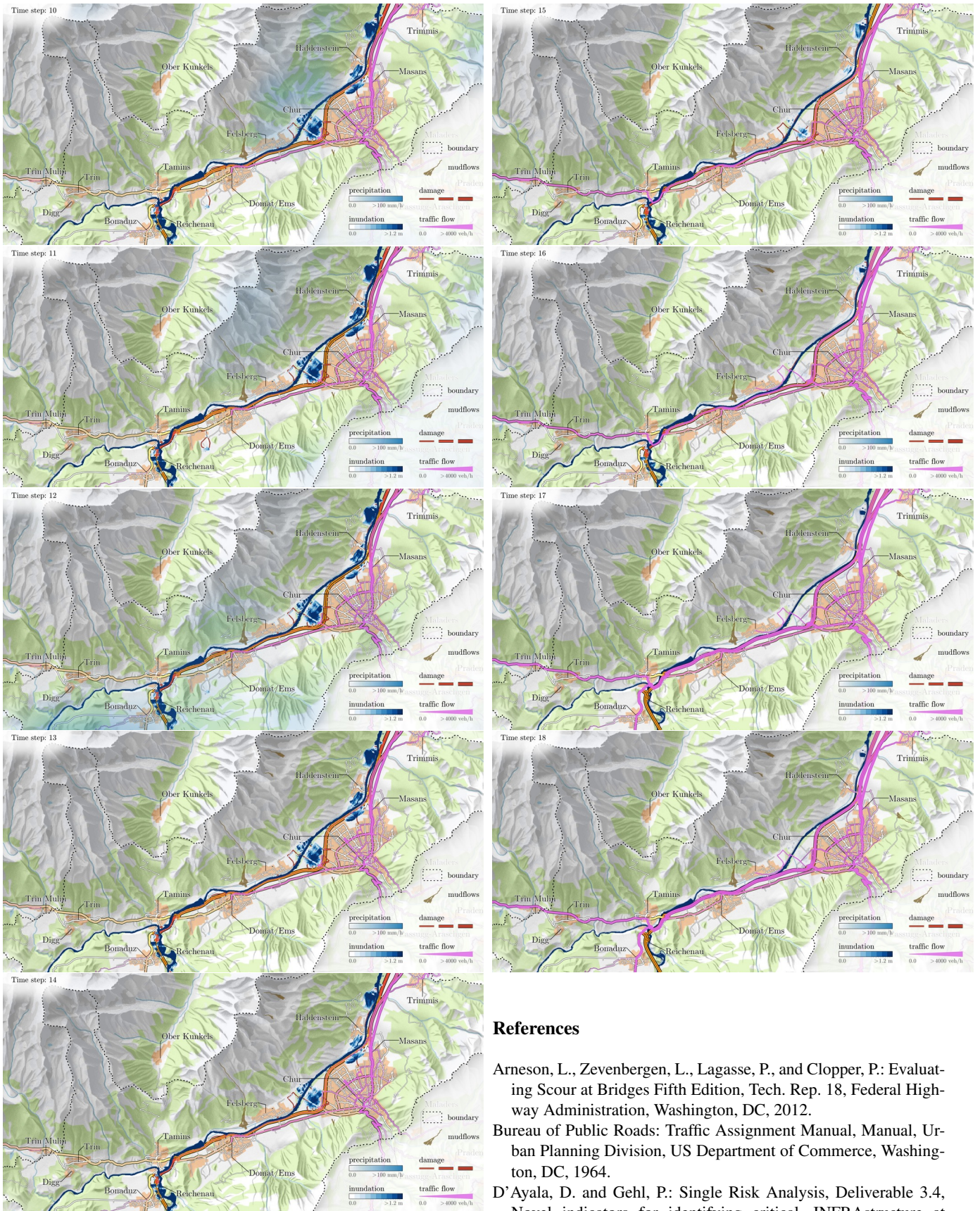
References

Arneson, L., Zevenbergen, L., Lagasse, P., and Clopper, P.: Evaluating Scour at Bridges Fifth Edition, Tech. Rep. 18, Federal Highway Administration, Washington, DC, 2012.

Bureau of Public Roads: Traffic Assignment Manual, Manual, Urban Planning Division, US Department of Commerce, Washington, DC, 1964.

D'Ayala, D. and Gehl, P.: Single Risk Analysis, Deliverable 3.4, Novel indicators for identifying critical, INFRAstructure at RISK from Natural Hazards (INFRARISK), 2015.

Feldman, A. D.: Hydrologic Modeling System HEC-HMS: Technical Reference Manual, Technical Report CPD-74B, US Army Corps of Engineers Hydrologic Engineering Center (HEC), Davis, CA, 2000.

Hackl, J., Heitzler, M., Lam, J. C., Adey, B. T., and Hurni, L.: Development of flood and mudflow events for the spatio-temporal risk assessment of networks, European Water, 57, 197–203, 2017.

Losey, S. and Wehrli, A.: Schutzwald in der Schweiz: Vom Projekt SilvaProtect-CH zum harmonisierten Schutzwald, Final report, Bundesamt für Umwelt (BAFU), Bern, Switzerland, 2013.

Pregnolato, M., Ford, A., Wilkinson, S. M., and Dawson, R. J.: The impact of flooding on road transport: A depth-disruption function, Transportation Research Part D: Transport and Environment, 55, 67–81, doi:10.1016/j.trd.2017.06.020, 2017.

Rickenmann, D.: Empirical Relationships for Debris Flows, Natural Hazards, 19, 47–77, doi:10.1023/A:1008064220727, 1999.

Roslan, N. I., Ghani, A. N. A., and Hamid, A. H. A.: Road subgrade strength under various flooding event, Jurnal Teknologi, 75, 39—-43, 2015.

Skempton, A. W. and Delory, F. A.: Stability of Natural Slopes in London Clay, pp. 378–381, Thomas Telford Publishing, London, UK, doi:10.1680/sposm.02050.0011, 1952.

Staubli, R. and Hirt, T.: Werterhalt von Strassen, Leitfaden für Politiker und Praktiker 1, Schweizerischer Gemeindeverband, Urtenen-Schönbühl, Switzerland, 2005.

VSS: Kosten-Nutzen-Analysen im Strassenverkehr: Zeitkosten im Personenverkehr, Swiss Standard SN 641 822a, Swiss Association of Road and Transport Experts (VSS), Zurich, Switzerland, 2009a.

VSS: Kosten-Nutzen-Analysen im Strassenverkehr: Betriebskosten von Strassenfahrzeugen, Swiss Standard SN 641 827, Swiss Association of Road and Transport Experts (VSS), Zurich, Switzerland, 2009b.

Walsh, I.: The Effects of Inundation on Pavements, Report 383, Jacobs, 2011.

Winter, M., Smith, J., Fotopoulou, S., Pitilakis, K., Mavrouli, O. C., Corominas Dulcet, J., and Argyroudis, S.: The physical vulnerability of roads to debris flows, in: International Symposium on Landslides, pp. 307–313, Taylor and Francis Group, Banff, 2013.

Wüest, M., Frei, C., Altenhoff, A., Hagen, M., Litschi, M., and Schär, C.: A gridded hourly precipitation dataset for Switzerland using rain-gauge analysis and radar-based disaggregation, International Journal of Climatology, 30, 1764–1775, doi:10.1002/joc.2025, 2010.

Zhang, Z., Wu, Z., Martinez, M., and Gaspard, K.: Pavement Structures Damage Caused by Hurricane Katrina Flooding, Journal of Geotechnical and Geoenvironmental Engineering, 134, 633–643, doi:10.1061/(ASCE)1090-0241(2008)134:5(633), 2008.

Zimmermann, M., Mani, P., and Gamma, P.: Murganggefahr und Klimaänderung - ein GIS-basierter Ansatz, NFP 31 Schlussbericht, vdf, Hochsch.-Verlag an der ETH, Zurich, Switzerland, 1997.